Applied Catalysis B: Environmental 158–159 (2014) 250–257

Contents lists available at ScienceDirect

Applied Catalysis B: Environmental

journal homepage: www.elsevier.com/locate/apcatb

Promoted effect of PANI as electron transfer promoter on CO oxidation over Au/TiO_2

Kai Yang, Kun Huang, Zhoujun He, Xun Chen, Xianzhi Fu, Wenxin Dai*

Research Institute of Photocatalysis, State Key Laboratory of Photocatalysis on Energy and Environment, Fuzhou University, Fuzhou 350002, China

ARTICLE INFO

Article history:
Received 6 February 2014
Received in revised form 20 March 2014
Accepted 15 April 2014
Available online 23 April 2014

Keywords:
CO oxidation
Electron transfer
Polyaniline
Au/TiO_2

ABSTRACT

Since a high electron density of Au surfaces can be conducive to the oxidation of CO over the supported Au nanoparticles, the conductive polymer polyaniline (PANI) was assembled into Au/TiO_2 to prepare a Au/TiO_2–PANI catalyst for oxidizing CO. It is found that PANI could be well wedged with Au/TiO_2, which remarkably promoted the oxidation of CO over the TiO_2 supported Au nanoparticles at room temperature. Moreover, the presence of a trace amount of H_2O could promote the oxidation of CO over the Au/TiO_2–PANI catalyst. Based on the testing results of structure characteristic, electrochemical impedance and adsorbing CO of Au/TiO_2–PANI, it was proposed that the PANI could be acted as an electron transmitter to promote the electron transfer from TiO_2 to Au, resulting in the increase of surface electron density of Au sites and then the promoted activation of CO adsorbed at Au sites.

1. Introduction

Supported gold catalysts deposited by the so-called deposition–precipitation method on the reducible TiO_2 (as an "active support") have been most extensively investigated and reported to exhibit thermal catalytic activity for CO oxidation at low temperature [1–8]. Although the fundamental reaction mechanism and the nature of the active sites associated with the high activity of oxide-supported Au catalysts are still not fully resolved and are growing debate, it is widely accepted that the high electron density of Au nanoparticles (i.e. negatively charged Au clusters) on "model" catalysts provides an active site and is beneficial to the oxidation of CO over Au catalysts [9–13]. On the one hand, a cluster anions (Au_n^-, with a higher electron density) can generate superoxo-like species via electron transfer to the LUMO of the O_2 molecule [14,15]; On the other hand, the surface electrons of Au can transfer to the π^* orbital of CO to promote the activation of CO [16,17]. For the TiO_2 supported Au catalyst, the reducible TiO_2 can donate electrons to Au nanoparticles by the Au/TiO_2 interface and then benefits to CO oxidation [18–20]. With this viewpoint, to build up a good interface of facilitating electron transfer to Au surfaces can be deemed as an effective pathway of promoting CO oxidation over Au/TiO_2.

Electrically conducting polymers, as a kind of good electrically conducting substance, have potential applications in catalysis and electron storage systems. The preparation of conducting polymers and gold nanoparticles has caused an increasing interest [21,22]. The polymers with a typical π–conjugated structure not only act as a stabilizer but also play a direct role to regulate the electronic structure of the Au clusters supported on it. The electrons donating effect of the storage electrons of the polymer matrices can transfer directly to the gold clusters referred to the covalent chemical bond binding between Au and π-delocalized conjugated N, O or S atoms of the polymers. For example, Tsunoyama et al. [23] obtained that the increase in the amount of negative charge on the Au core stabilized by polyvinylphenol (PVP) could donate more electronic charges to CO molecule, resulting in a higher activity toward aerobic oxidation. The polyaniline (PANI) with the delocalized π-conjugated structure is one of the most extensively studied conducting polymers and has been widely investigated for electronic application due to both its good environmental stability and tunable electrical properties. Moreover, it has intriguing properties with benzenoid and quinonoid units and has several redox states [24]. This indicates that PANI may be acted as electron transfer promoter when introduced into Au catalyst.

Thus, in this work the electrically conducting polymer (PANI) is introduced into the Au/TiO_2 system for oxidizing CO at room temperature. It is expected that the collective advantages of Au nanoparticles, TiO_2 and PANI can be combined to construct ternary materials with well-defined structures, composition, catalytic activity as well as electron storage and transfer trait. It is

* Corresponding author. Tel.: +86 591 83779083; fax: +86 591 83779083.
E-mail address: daiwenxin@fzu.edu.cn (W. Dai).

http://dx.doi.org/10.1016/j.apcatb.2014.04.028
0926-3373/

found that this assembly structure really make a synergetic effect on the oxidation of CO at room temperature.

2. Experimental

2.1. Preparation of catalysts

Au/TiO_2–PANI catalysts were prepared by the in situ polymerization of aniline in the present of TiO_2 nanoparticles followed by loading gold via the deposition–precipitation method step by step.

The prepared TiO_2 sol [25] was dried at 80 °C and calcined at 450 °C for 3 h to prepare TiO_2 powder. 2 g of TiO_2 and 50 μL aniline were dispersed in the 80 mL of 1 mol L^{-1} HCl solution. After stirred vigorously for 30 min at room temperature, a solution of 10 mL water and 2.45 g ammonium persulfate was added dropwise to the above solution with a buret under magnetic stirring. The resultant mixed suspension was stirred for 5 h and filtered, after which the slurry was washed with deionised water several times and dried overnight in an oven at 80 °C. Based on the theoretical calculation, this prepared powder sample was denoted as TiO_2–PANI (40:1) (the weight ratio of TiO_2 to PANI). Following the above steps, TiO_2–PANI (20:1) and TiO_2–PANI (10:1) were also prepared by in situ polymerization of 100 and 200 μL aniline in the presence of ammonium persulfate oxidant, respectively.

Au-supported TiO_2 and TiO_2–PANI were synthesized according to a classic deposition–precipitation method. 0.02 g of $HAuCl_4{\cdot}3H_2O$ was added into 20 mL deionized water, and then the above TiO_2 or TiO_2–PANI support was added, with vigorous stirring, into the solution. After stirred at room temperature for 30 min, the pH value of the resulting gold precursor slurry was adjusted to 10 with 1.0 mol L^{-1} NaOH aqueous solution at room temperature. This was followed by washing with water several times, until a test by $AgNO_3$ no longer showed the presence of residual Cl^-. The obtained particles were dispersed in the 20 mL deionized water and reduced using a 1.0 mol L^{-1} $NaBH_4$ aqueous solution at room temperature. The products were washed with water for 3 times and were dried at 80 °C overnight to yield the as-synthesized samples (i.e., Au/TiO_2, Au/TiO_2–PANI (40:1), Au/TiO_2–PANI (20:1) and Au/TiO_2–PANI (10:1)). The loading amount of Au for all the samples is about 1.0 wt%.

2.2. Characterization of catalysts

X-ray diffraction (XRD) pattern was recorded on a Bruker D8 Advance powder X-ray diffractometer using Cu *Kα* radiation (λ = 0.15418 nm) operated at 40 kV and 40 mA. The microstructures of the samples were determined by using an SU8000 (Hitachi) scanning electron microscope (SEM). Transmission electron microscopy (TEM) investigation together with an electron-diffraction image was carried out on a JEOL JEM-2010 EX with field emission gun at 200 kV. Energy dispersive X-ray (EDX) spectrum was also obtained with an EDX spectrometer (USA, EDax instrument). Raman spectra were taken on LabRAM HR UV-NIR Microscope (HORIBA Jobin Yvon) employing a 532 nm excitation of Ar^+ ion laser. XPS was performed at a Quantum2000 system. XPS data were collected using the Al *Kα* X-ray beam (1486.6 eV) operated at 25 W. The C 1s signal of 284.6 eV was used for the calibration of XPS data. The electrochemical impedance spectroscopy (EIS) measurements were carried out by using three-electrode cells. The resultant electrode served as the working electrode, with a platinum wire as the counter electrode and a Ag/AgCl (saturated KCl) electrode as the reference electrode. The working electrodes were prepared as follows: 10 mg grinded sample was added to 5 mL absolute ethanol to make slurry. The slurry was then injected onto a 2.5 cm × 1.0 cm FTO glass with the cell size of 5 mm × 5 mm and they were dried at 80 °C for 120 min.

2.3. Catalytic performance

Catalytic oxidation of CO was conducted in a fixed-bed flow reactor at atmospheric pressure using 500 mg of catalyst at a total flow rate of 100 mL min^{-1}. Catalyst sample with a grain size of 0.2–0.3 mm was placed in a square quartz cell with a cooling water system. The feed stream contained 0.3 vol% CO, 0.3 vol% O_2 and a balance He. The temperature of the quartz cell was controlled at about 25 °C (measured by a thermocouple placed inside the catalyst bed). For the effect of water on CO oxidation, the feed stream went through different supersaturated solution with different relative humidity (RH) in advance, respectively (LiCl (RH) = 13%, K_2CO_3 (RH) = 43%, $Mg(NO_3)_2$ (RH) = 54%, NaCl (RH) = 75%, KCl (RH) = 85%, KNO_3 (RH) = 90%).

2.4. CO adsorption of catalysts

Fourier transform infrared spectra (FT-IR) of CO adsorption at room temperature were conducted on the atmospheric pressure in the infrared cell reactor and recorded after exposure of the samples to bare CO until a steady state for 30 min was reached. Prior to the admittance of CO, background spectra were recorded. The samples were pressed into a holder fitted with an aluminum foil and placed in the vacuum cell. The samples were pretreated for 2 h at 150 °C.

3. Results and discussions

3.1. Catalyst characterization

3.1.1. XRD

Fig. 1 shows the representative XRD patterns of TiO_2, Au/TiO_2 and Au/TiO_2–PANI with different mole ratios of TiO_2 and PANI. For the bare TiO_2, all the diffraction peaks can be indexed as the typical anatase phase of TiO_2 in agreement with the values in the standard card (JCPDS file no. 21-1272). Diffraction peaks at 2θ values of 25.3, 37.8, 48.0, 53.9 and 62.7, can be corresponded to the (1 0 1), (0 0 4), (2 0 0), (1 0 5) and (2 0 4) crystallographic planes of anatase TiO_2, respectively. The XRD patterns of TiO_2 and TiO_2–PANI after loading Au show that the peak at 2θ = 38.2° can be indexed to the (111) face of Au (JCPDS file no. 65-2870) [26], demonstrating the existence of Au nanoparticles. Moreover, the peak of the PANI samples centered at 2θ = 27.5° can be attributed to the periodicity of PANI chain [27], indicating the formation of the polymer.

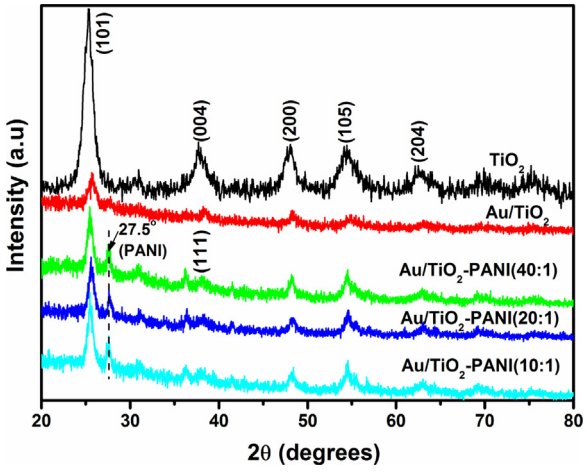

Fig. 1. XRD patterns of TiO_2, Au/TiO_2 and Au/TiO_2–PANI samples.

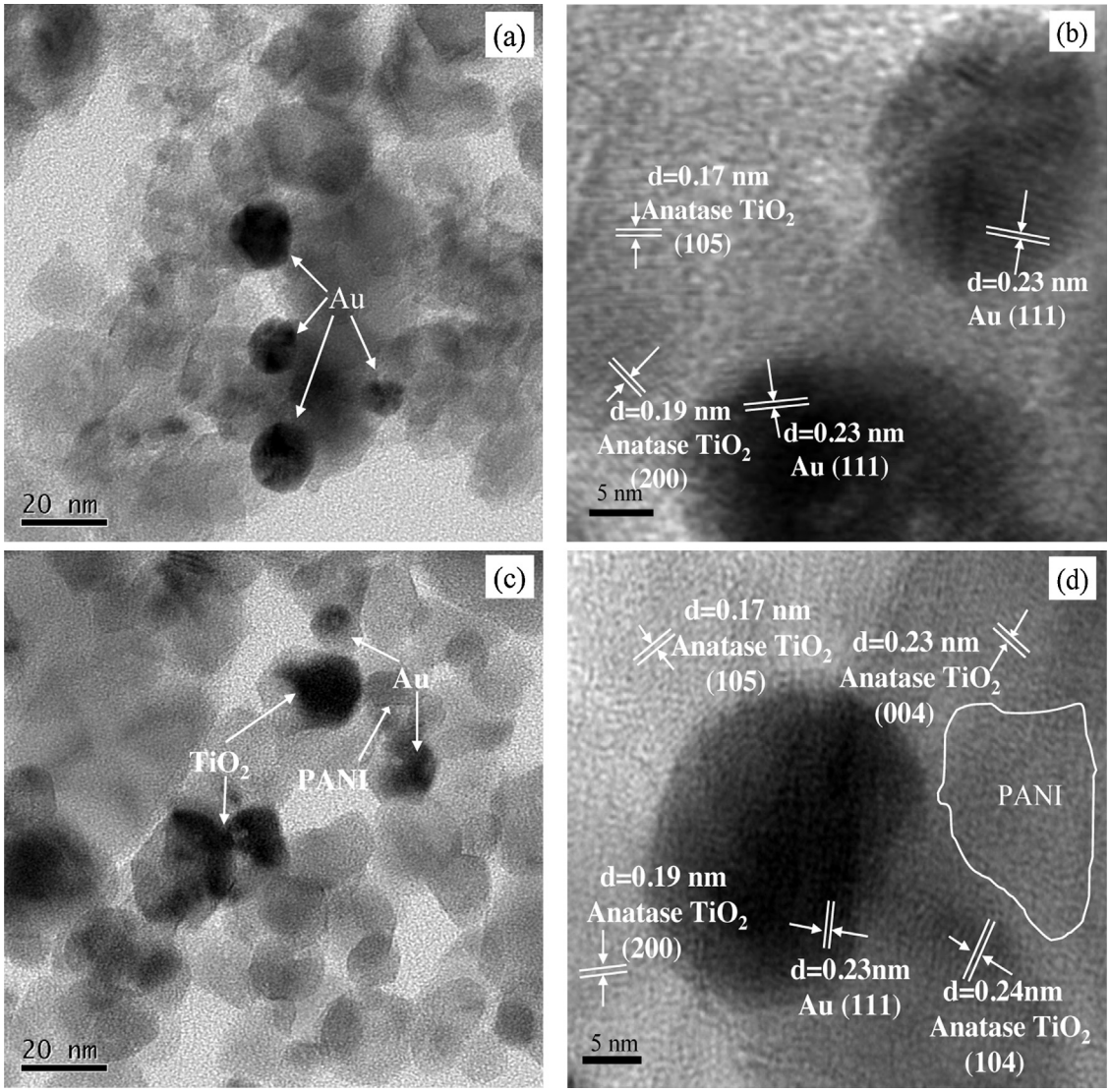

Fig. 2. TEM images of Au/TiO_2 (a and b) and Au/TiO_2–PANI (20:1) (c and d) samples.

Moreover, Au/TiO_2–PANI shows a good stability below 450 °C (seen in supporting information 1 (SI1)).

3.1.2. Electron microscope analysis

The SEM images show that Au/TiO_2–PANI (20:1) exhibits a similar morphology to Au/TiO_2, displaying a loose morphology and large irregular non-uniform particles in the main textural phase (seen in SI2). This loose architecture may be contributive to the mass transfer, adsorption and activation of reactant gases arriving at the catalytic active sites. Moreover, the TEM images in Fig. 2 show that both Au/TiO_2 and Au/TiO_2–PANI (20:1) have almost the same Au particle size distribution (a vs. c) with the range of 10–20 nm (b vs. d). This indicates that the immobilization process does not affect the size of the Au nanoparticles. Thus, in this case the difference in activity of the two catalysts can be mainly attributed to the difference in the chemical architecture and composition. Meanwhile, EDX result (seen in SI3) also manifests that Au nanoparticles and PANI were well-anchored onto the reducible TiO_2 support.

3.1.3. Raman spectra

To certify the interaction among TiO_2, PANI and Au in Au/TiO_2–PANI samples, the Raman spectra of the TiO_2, Au/TiO_2 and Au/TiO_2–PANI were performed in the range 100–1700 cm^{-1}.

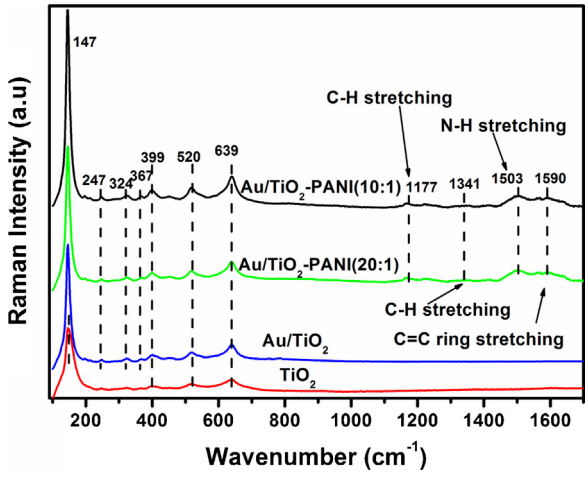

Fig. 3. Raman spectra of TiO_2, Au/TiO_2 and Au/TiO_2–PANI samples.

As shown in the Fig. 3, the four bands located at about 147 (E_{1g}), 399 (B_{1g}), 520 (A_{1g} +B_{1g}), and 639 cm^{-1} (E_{1g}) can be assigned to the characteristic vibration peaks for anatase TiO_2 [28]. After Au loading into TiO_2, the three emerging vibration peaks located at

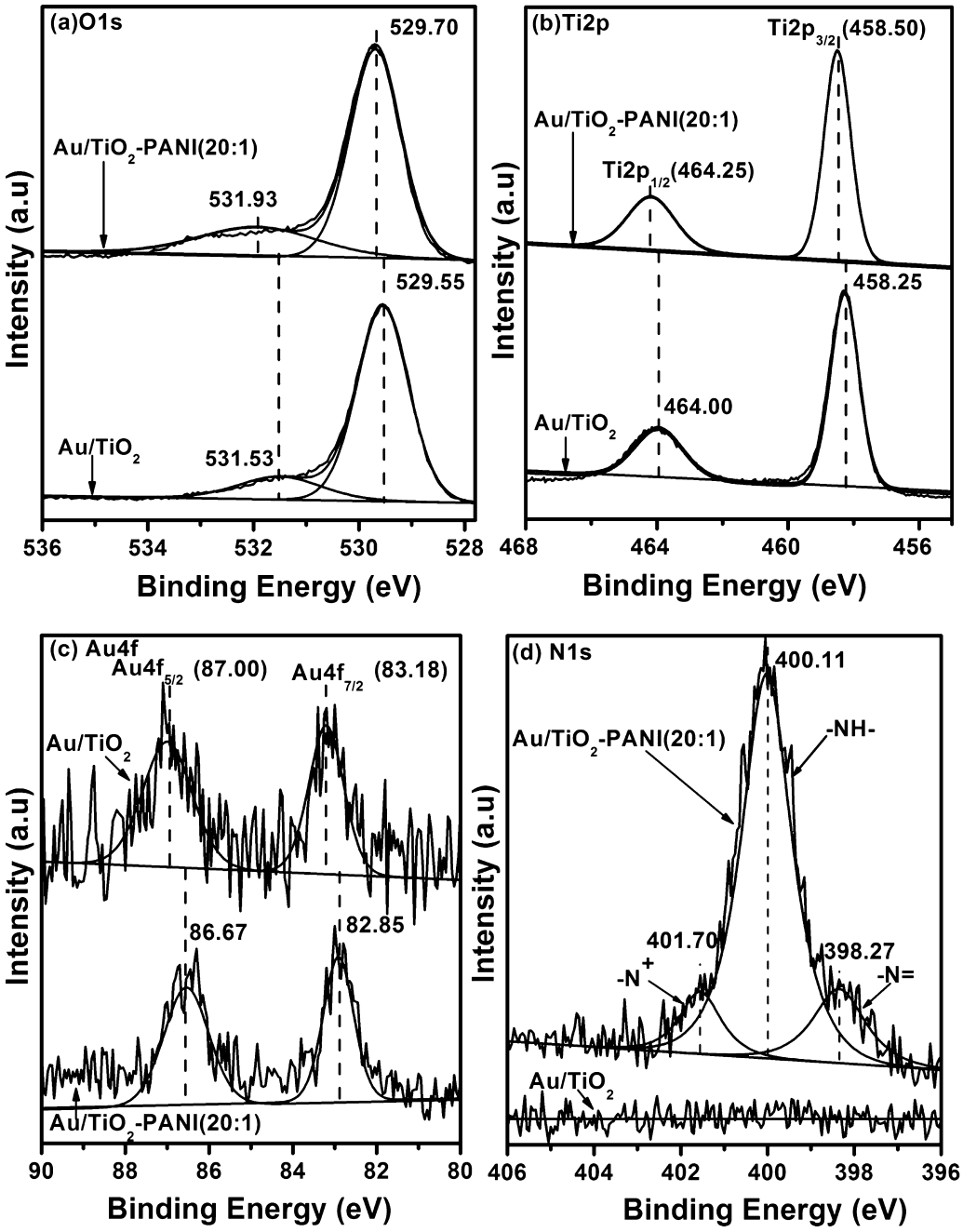

Fig. 4. High-resolution XPS spectra of Au/TiO_2 and Au/TiO_2–PANI (20:1): (a) O1s, (b) Ti2p, (c) Au4f, and (d) N1s.

about 247, 324 and 367 cm^{-1} are observed, which may be deemed as the characteristic of Ti—O—Au bond [29]. This observation verifies the joint introduction of gold and TiO_2 into the nanocomposites. Moreover, with the introduction of PANI into Au/TiO_2, the characteristic band vibrations of PANI (the vibrations are sensitive to the structure of polyaniline) are observed in the Raman spectra. The band at 1590 cm^{-1} can be assigned to the C—C stretching vibration of the benzenoid or quinoid rings [30]. The bands at 1503 and 1341 cm^{-1} correspond to the protonated C=N^+ stretching mode and the protonated C—N^+ stretching of the delocalized polaronic charge carriers [31], respectively. In addition, the band at 1177 cm^{-1} can be attributed to the C—H bending of the quinoid ring and benzenoid ring. However, all the Raman bands for anatase TiO_2 and PANI are basically retained in Au/TiO_2–PANI samples. Note that the presence of Au nanoparticles significantly increases the intensity of the characteristic Raman bands of TiO_2 compared with the bare TiO_2 and the co-existence of PANI and Au further increases that. This may be resulted from two reasons: One may be that the nanoscale roughness [32] of Au/TiO_2 or Au/TiO_2–PANI brings about the effect of surface enhanced Raman scattering, the other may be the promotion of charge transfer among gold nanoparticles, PANI and TiO_2 [33]. In this case, TiO_2 with partially positively charge and gold nanoparticles with partially negatively charge can be cohesive together. This indicates that the introduction of PANI maybe promote the electron transfer from TiO_2 to Au. To confirm it, XPS testing was performed to further identify the surface states of Au, C, O, Ti and N atoms in Au/TiO_2–PANI.

3.1.4. XPS

As seen in Fig. 4a, the O1s XPS spectra of Au/TiO_2 and Au/TiO_2–PANI (20:1) can be deconvoluted into two peaks, where the peak at a binding energy (BE) of 529.51 eV can be assigned to the

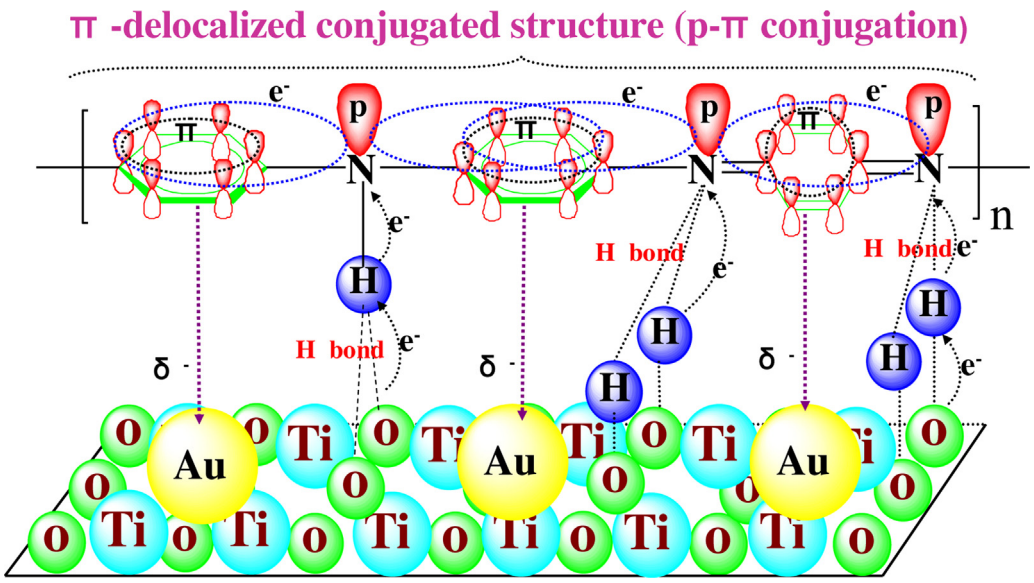

Scheme 1. A schematic illustration showing the possible process of electron transfer over the well-attached Au/TiO_2–PANI system. Here, PANI can accept electrons from TiO_2 by the hydrogen bonds (TiO_2—O. . .HN—PANI), and donate the captured electrons to Au nanoparticles by the structure of p-π-delocalized conjugated benzenoid or quinonoid units with N atoms in PANI.

lattice oxygen in the anatase phase of TiO_2 [34] and the other peak at 531.62 eV corresponds to the oxygen species in the Ti—OH hydroxyl group. Note that the oxygen species resulting from the lattice oxygen and the surface hydroxyl groups (Ti—OH) of Au/TiO_2–PANI exhibit a pronounced BE shift of 0.15 eV (from 529.55 to 529.70 eV) and 0.40 eV (from 531.53 to 531.93 eV) in comparison with that of Au/TiO_2, respectively. This indicates that the coordination process of the imine groups (—N=) of PANI with the surface hydroxyl groups of Au/TiO_2 (Ti—OH) is accessible. In addition, the lattice oxygen of the TiO_2 is also probably participated into the bonding reaction with the amine groups (—NH—) of PANI by the formation of copious hydrogen bond network (TiO_2—O. . .HN—PANI) (shown in Scheme 1) during the assembly process of the polymerization of anline [35]. So it can build the further well-dispersed assembly of Au nanoparticles on the TiO_2–PANI support by electrostatic interaction between PANI and TiO_2 (the electrons transfer from TiO_2 to PANI due to the positive shift of O1s). Moreover, the BE values of Ti $2p_{3/2}$ (458.50 eV) or Ti $2p_{1/2}$ (464.25 eV) of Au/TiO_2–PANI exhibit positive shifts of 0.25 eV compared to those of Ti$2p_{3/2}$ (458.25 eV) or Ti$2p_{1/2}$ (464.00 eV) of Au/TiO_2 (Fig. 4b). This also indicates that the introduction of PANI reduces the surface electron density of TiO_2. Since the oxygen defect of TiO_2 surfaces can result in the electron migration from TiO_2 to the adjacent Au sites over the TiO_2 supported Au nanoparticles [36], it is easily supposed that the reduced electrons from TiO_2 maybe transfer to Au nanoparticles.

Fig. 4c shows the Au 4f XPS spectra of Au/TiO_2 and Au/TiO_2–PANI (20:1). The Au $4f_{7/2}$ and Au $4f_{5/2}$ spin-orbital splitting photoelectrons are located at the characteristic peaks of BE of 83.18 and 87.00 eV of Au/TiO_2, indicating that Au nanoparticles of Au/TiO_2 are almost reduced to zero-valent metallic Au. With respect to that of bulk metallic Au (84.10 eV), a negative shift of BE for 0.90 eV to lower values is observed. Therefore, Au/TiO_2 itself has the strong electron transfer from TiO_2 support to Au nanoparticles [37]. After loading PANI, the Au $4f_{7/2}$ spin-orbital splitting photoelectrons for Au/TiO_2–PANI (20:1) is located at BE of 82.85 eV, which exhibiting a negative shift of 0.33 eV to lower BE compared to that of Au/TiO_2. Similarly to our result, a negative shift up to 0.30 eV for BE have been reported for Pt clusters stabilized by poly (N-vinyl-2-pyrrolidone) and gold nanoparticles stabilized by β-cyclodextrin [38]. The larger negative-shift of Au BE of Au/TiO_2–PANI (20:1) suggests that the electrons indeed transfer from TiO_2 to Au nanoparticles by PANI. Maybe, the strong interaction between PANI and TiO_2 holds the electron density of Au nanoparticles.

Fig. 4d shows the N 1s binding energy region of the Au/TiO_2 and Au/TiO_2–PANI. It is observed that three different nitrogen environments are present in this case: the two lower BE peaks (398.27 and 400.11 eV) correspond to the benzenoid diamine (—NH—) and the quinoid remain-diimine species (—N=), respectively; the other peak at 401.70 eV should be assigned to the protonated amine or imine species ($—N^+$) [39]. The percentage of N_{amine}, N_{imine} and $—N^+$ are of about 8.0%, 87.0% and 5.0%, respectively. As a better electron transfer and highly conductive state, PANI can achieve it through the protonation of the —N= or the oxidation of the —NH—. In this work, the observed peak at 401.70 eV means that the —N= of PANI is protonated by the surface hydroxyl groups of TiO_2 or the —NH— of PANI interacts with the lattice oxygen of TiO_2 by interchain H-bonding (Scheme 1). Besides, due to the oxidability of Au, PANI can be also oxidized, resulting in the trace change of —NH— to $—N^+$ groups. In this case, PANI can achieve its highly conductive state either through the protonation of the imine nitrogens (—N=) or through the oxidation of the amine nitrogens (—NH—) [40]. Therefore, these observations of changes in polymer state indicate charge storage and transfer capacity of PANI [41]. That is to say, the different valent states of N atoms maybe take part in the process of electron transfer from TiO_2 to Au nanoparticles. As a matter of fact, the polymers with a typical π-conjugated structure can donate the storage electrons of the polymer matrices to the gold clusters referred to the covalent chemical bond binding between Au and π-delocalized conjugated N, O or S atoms of the polymers [21–23]. In addition, the different states of N atoms can be also shown by the C1s core level XPS spectrum of Au/TiO_2–PANI (seen in SI4).

Based on the above synergetic investigations of FT-IR spectra, Raman spectra, XPS, the bonding mechanism of PANI assembled into the Au/TiO_2 system is proposed in Scheme 1. On the one hand, PANI can accept electrons from TiO_2 by the hydrogen bonds (TiO_2—O. . .HN—PANI); On the other hand, the captured electrons can transfer to the Au nanoparticles by the covalent chemical bond binding between Au and the p-π-delocalized conjugated N atom (formed by the p orbital of N atom with the π-delocalized conjugated benzenoid or quinonoid unit). It may be the two attractive

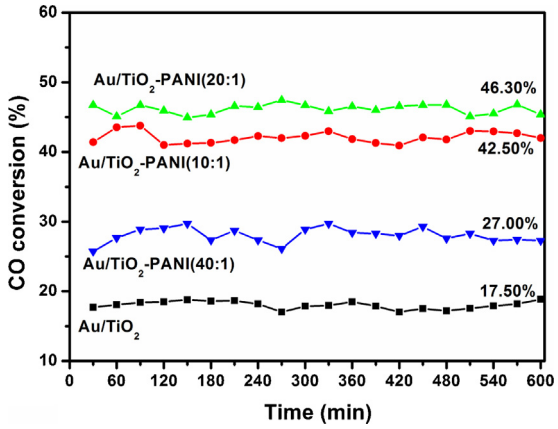

Fig. 5. CO conversions as function of reaction time over Au/TiO_2 and Au/TiO_2–PANI samples.

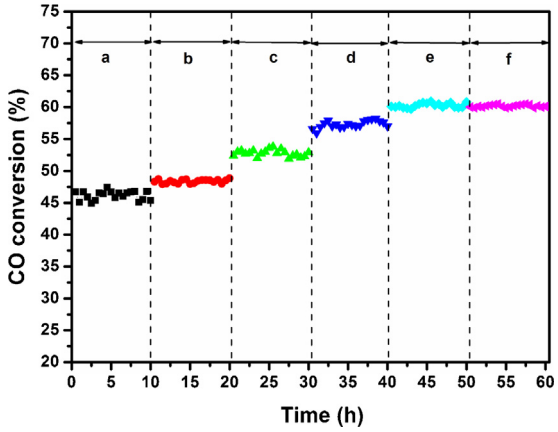

Fig. 6. CO conversions over Au/TiO_2–PANI (20:1) as a function of reaction time during the different moisture concentrations: (a) RH = 13%, (b) RH = 43%, (c) RH = 54%, (d) RH = 75%, (e) RH = 85%, (f) RH = 90%.

forces to promote the electron transfer from TiO_2 to PANI to Au nanoparticles, which finally result in an excellent catalytic performance.

3.2. Catalytic performances

Fig. 5 shows the catalytic performances of Au/TiO_2 and Au/TiO_2–PANI toward CO oxidation. In comparison, it is clear that the single Au/TiO_2 exhibits a lower activity for CO oxidation, where a 17.50% conversion of CO is reached at ambient temperature. After the loading of PANI, all the Au/TiO_2–PANI composite catalysts show higher activity for oxidizing CO than the initial Au/TiO_2. Hereinto, the Au/TiO_2–PANI (20:1) exhibits the highest conversion of CO (46.30%), which is more twice than that of Au/TiO_2. However, the more addition of PANI into Au/TiO_2 will decrease the conversion of CO (42.50% over Au/TiO_2–PANI (10:1)). This result indicates that the addition of the optimum PANI can markedly promote the catalytic activity of Au/TiO_2 for oxidizing CO.

As a matter of fact, there is more or less some moisture for the feed gas of oxidizing CO in a real application environment. For this, moisture with different relative humidity was introduced into the feed gases to estimate the activity of oxidizing CO over Au/TiO_2–PANI (20:1). As depicted in Fig. 6, the gradual change in H_2O concentration with different relative humidity causes the ladder-type rise of the activity. It indicates that the trace amount of H_2O can promote the catalytic activity of Au/TiO_2–PANI (20:1) and reach to a stable CO conversion (60.30%) up to the relative

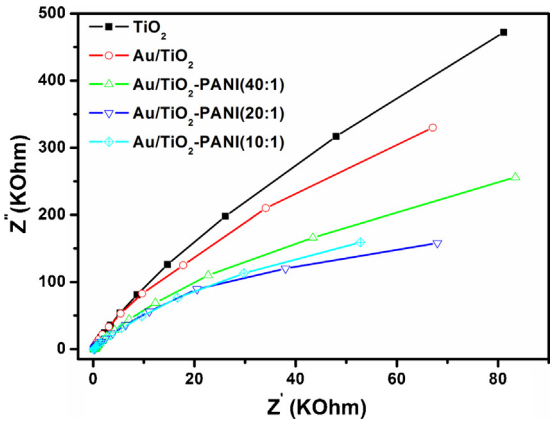

Fig. 7. EIS Nyquist plots of Au/TiO_2 and Au/TiO_2–PANI electrodes, the amplitude of the sinusoidal wave was set at 10 mV and the frequency varied from 100 kHz to 0.05 Hz.

humidity (RH) at 85%, which is consistent with that over Au/TiO_2 reported by Haruta et al. [42]. Moreover, our previous research [43] has also indicated that at or below 80 °C the oxidation of CO over Au/TiO_2 involves a reaction with related to water-derived species on the catalyst surface in the stream containing a trace amount of H_2O. This result shows that the presence of a trace amount of H_2O does not suppress the promoted effect of PANI on CO oxidation over Au/TiO_2. This also means that this prepared Au/TiO_2–PANI catalyst may be applied under a real environment condition.

3.3. Discussion

According to the analysis of XPS, the introduction of PANI can promote the electron transfer from TiO_2 to Au. In order to further reveal it, a EIS electrochemical performance measurement on the impedance changes of the modified electrode surface was adopted to evaluate the efficiency of interface charge transfer and separation for catalytic performance [44]. Proposed circuit by indium-tin oxide (ITO)/TiO_2 or ITO/Au/TiO_2 or ITO/Au/TiO_2–PANI as the working electrode and platinum flake as a counter electrode with a saturated calomel electrode as a reference electrode was constructed with serial combination of bulk electrolyte resistance, interfacial reaction impedance, and inner surface charge transfer impedance [45]. Here, interfacial reaction impedance is extremely minute and can be ignored. For different samples, electrolyte resistance is identical under the same measurement condition. Thus, to compare EIS Nynquist plots of all the samples, the radius of the semiarc reflects inner surface charge transfer rate occurring at the catalysts. The smaller size of the semiarc in an EIS Nyquist plots indicates the smaller resistance at the interface of materials and the smaller charge-transfer resistance on the electrode surfaces [46]. Fig. 7 shows the Nyquist plots of TiO_2, Au/TiO_2 and Au/TiO_2–PANI electrodes. The size of the semiarc radius on the Nyquist plot of the Au/TiO_2 electrode is smaller than that of the bare TiO_2 electrode. It reveals that the interfacial transfer of carriers between Au and TiO_2 is well-achieved. After the incorporation with PANI, the semicircle switchs smaller, indicating that the more surface electron transfer is achieved (the Au/TiO_2–PANI (20:1) with the smallest resistance shows the most surface electron transfer behavior). As can be seen, the Au/TiO_2–PANI hybrid structure indeed induces the effect of better efficient electron transfer and charge separation compared with those of Au/TiO_2 binary composite and bare TiO_2.

This above efficient electron transfer finally causes the increase in surface electron density of Au nanoparticles, which promotes the adsorption of CO at Au sites and its activation. To confirm it, the FT-IR spectra of CO absorption were recorded to investigate the

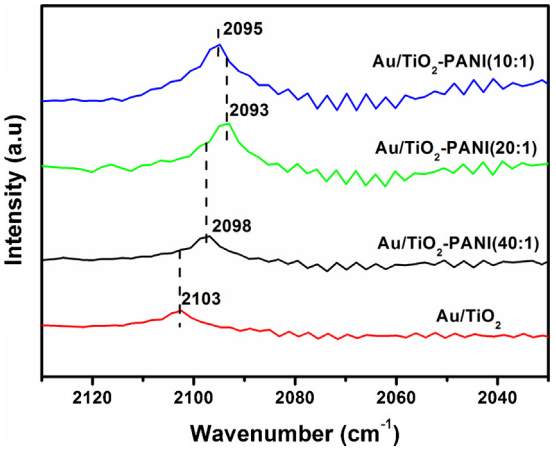

Fig. 8. FT-IR adsorption spectra of Au/TiO_2 and Au/TiO_2–PANI samples after adsorbing CO, respectively.

adsorption behaviors of CO at Au sites of Au/TiO_2 and Au/TiO_2–PANI (seen in Fig. 8). When CO is added into Au/TiO_2 at the vaccum environment, the absorption at 2103 cm^{-1} is observed, which is assigned to the line chemisorption of CO at the low-coordination sites of metallic Au sites [47]. With the introduction of PANI, a larger CO peak with a lower frequency (<2103 cm^{-1}) is observed, indicating that the more CO molecules with a relative active state are adsorbed at Au sites [48]. Hereinto, the Au/TiO_2–PANI (20:1) shows the lowest frequency at 2093 cm^{-1} (the optimum activation of CO). However, the excessive amount of PANI (Au/TiO_2–PANI (10:1)) can suppress the adsorption of CO and its activation at Au sites.

Further comparing the results of both EIS (Fig. 7) and adsorbing CO (Fig. 8) of each sample with its activity (Fig. 5), it is found that the Au/TiO_2–PANI (20:1) with the lowest resistance shows the highest activation extent of CO adsorbed at Au sites and the highest activity of oxidizing CO. This means that the promoted effect of PANI on oxidizing CO over Au/TiO_2–PANI can be mainly attributed to the increase in surface electron density of Au nanoparticles induced by the promoted electron transfer of PANI. This result also shows that the oxidation of CO over Au/TiO_2–PANI is mainly dependent on the activation of CO at Au sites, consistent with the report by Liu et al. [49].

Based on the above results and analysis, it is suggested that PANI may be acted as an electron transmitter to promote the electrons from TiO_2 to Au sites. The probable process of PANI promoting CO oxidation over Au/TiO_2–PANI can be proposed as follows:

$$TiO_2(Ti^{3+}(e)) + PANI \rightarrow TiO_2(Ti^{4+}) + PANI(e) \quad (1)$$

$$PANI(e) + Au \rightarrow PANI + Au^{\delta-} \quad (2)$$

$$Au^{\delta-} + CO \rightarrow \{Au{-}C{=}O\} \quad (3)$$

$$TiO_2(Ti^{3+}(e)) + O_2 \rightarrow TiO_2{-}O_2^- \quad (4)$$

$$2\{Au{-}C{=}O\} + TiO_2{-}O_2^- \rightarrow 2Au + 2CO_2 + TiO_2(e) \quad (5)$$

During the above processes, PANI first accepts the electrons from TiO_2 (oxygen vacancy electrons) by the hydrogen bonds (TiO_2—O. . .HN—PANI) (Reaction (1)). Then the captured electrons transfer into the Au nanoparticles by the covalent chemical bond binding between Au and the p-π-delocalized conjugated N atoms (Reaction (2)), resulting in the increase of surface electron density of Au nanoparticles. These Au sites with rich-electrons can benefit to the adsorption of CO and its activation (Reaction (3)), which then reacts with the O_2^- adsorbed at TiO_2 sites adjacent to Au sites (Reaction (4)) to form CO_2 (Reaction (5)). Of course, the PANI maybe also exert an influence on the adsorption of O_2 and its activation during the reaction process. However, the promotion of CO oxidation induced by O_2 activation is probably less than that induced by CO activation [43].

4. Conclusions

In summary, the Au/TiO_2–PANI ternary composites prepared by an insitu polymerization and the following deposition–precipitation method, exhibit a higher activity of oxidizing CO than Au/TiO_2. Moreover, the presence of a trace amount of H_2O does not suppress the promoted effect of PANI on CO oxidation over the TiO_2 supported Au catalyst. The results of the structure analysis, EIS experiment and FT-IR testing of adsorbing CO of Au/TiO_2–PANI, show that PANI can be acted as an electron transmitter (due to the structure of p-π-delocalized conjugated N atoms with benzenoid or quinonoid unit) to promote the electron transfer from TiO_2 to Au nanopaticles, resulting in the increase of surface electron density of Au sites and then the promoted activation of CO at Au sites. This study maybe provide a promising approach to extend other conducting polymers in the environmental purification of oxidizing CO at room temperature and even in other thermocatalytic reactions.

Acknowledgments

This work was financially supported by the National Natural Science Foundation of China (nos. 21073037 and 21273037) and the National Basic Research Program of China (973 Program, no. 2014CB239303).

Appendix A. Supplementary data

Supplementary data associated with this article can be found, in the online version, at http://dx.doi.org/10.1016/j.apcatb.2014.04.028.

References

[1] G.C. Bond, C. Louis, D.T. Thompson, Catalysis by Gold: Catalytic Science Series 6, IC (Imperial College) Press, London, Great Britain, 2006, pp 1–366.
[2] B. Hammer, J.K. Nørskov, Nature 376 (1995) 238–240.
[3] M. Daté, H. Imai, S. Tsubota, M. Haruta, Catal. Today 122 (2007) 222–225.
[4] G.J. Hutchings, M.S. Hall, A.F. Carley, P. Landon, B.E. Solsona, C.J. Kiely, A. Herzing, M. Makkee, J.A. Moulijn, A. Overweg, J.C. Fierro-Gonzalez, J. Guzman, B.C. Gates, J. Catal. 242 (2006) 71–81.
[5] H. Fan, C. Shi, X. Li, S. Zhang, J. Liu, A. Zhu, Appl. Catal. B 119/120 (2012) 49–55.
[6] M. Daté, M. Okumura, S. Tsubota, M. Haruta, Angew. Chem. Int. Ed. 43 (2004) 2129–2132.
[7] L. Piccolo, H. Daly, A. Valcarcel, F.C. Meunier, Appl. Catal. B 86 (2009) 190–195.
[8] M. Haruta, S. Tsubota, T. Kobayashi, H. Kageyama, M. Jenet, B. Delmon, J. Catal. 144 (1993) 175–192.
[9] L. Fan, N. Ichikuni, S. Shimazu, U. Takayoshi, Appl. Catal. A: Gen. 246 (2003) 87–95.
[10] H. Hakkinen, U. Landman, J. Am. Chem. Soc. 123 (2001) 9704–9705.
[11] M. Okumura, Y. Kitagawa, M. Haruta, K. Yamaguchi, Chem. Phys. Lett. 346 (2001) 163–168.
[12] D.C. Meier, D.W. Goodman, J. Am. Chem. Soc. 126 (2004) 1892–1899.
[13] A. Sanchez, S. Abbet, U. Heiz, W.D. Schneider, H. Hakkinen, R.N. Barnett, U. Landman, J. Phys. Chem. A 103 (1999) 9573–9578.
[14] B. Yoon, H. Hakkinen, U. Landman, J. Phys. Chem. A 107 (2003) 4066–4071.
[15] L.M. Molina, B. Hammer, J. Chem. Phys. 123 (2005) 161104.
[16] J.A. Van Bokhoven, C. Louis, J.T. Miller, M. Tromp, O.V. Safonova, P. Glatzel, Angew. Chem. Int. Ed. 45 (2006) 4651–4654.
[17] N. Weiher, A.M. Beesley, N. Tsapatsaris, L. Delannoy, C. Louis, J.A. Van Bokhoven, S.L.M. Schroeder, J. Am. Chem. Soc. 129 (2007) 2240–2241.
[18] M. Chen, Y. Cai, Z. Yan, D.W. Goodman, J. Am. Chem. Soc. 128 (2006) 6341–6346.
[19] M. Haruta, Gold Bull. 37 (2004) 27–36.
[20] I.N. Remediakis, N. Lopez, J.K. Nørskov, Angew. Chem. Int. Ed. 44 (2005) 1824–1826.
[21] K. Huang, Y. Zhang, Y. Long, J. Yuan, D. Han, Z. Wang, L. Niu, Z. Chen, Chem. -Eur. J. 12 (2006) 5314–5319.
[22] X. Sun, S. Dong, E. Wang, Chem. Commun. 10 (2004) 1182–1183.
[23] H. Tsunoyama, N. Ichikuni, H. Sakurai, T. Tsukuda, J. Am. Chem. Soc. 131 (2009) 7086–7093.
[24] E.T. Kang, K.G. Neoh, K.L. Tan, Prog. Polym. Sci. 23 (1998) 277–324.

[25] X.H. Lin, K. Yang, R.R. Si, X. Chen, W.X. Dai, X.Z. Fu, Appl. Catal. B 147 (2014) 585–591.
[26] K. Yan, G.S. Wu, C. Jarvis, J.L. Wen, A.C. Ch, Appl. Catal. B 148/149 (2008) 281–287.
[27] G. Sonmez, H.B. Sonmez, C.K.F. Shen, F. Wudl, Adv. Mater. 16 (2004) 1905–1908.
[28] S.M. Miranda, G.E. Romanos, V. Likodimos, R.R.N. Marques, E.P. Favvas, F.K. Katsaros, K.L. Stefanopoulos, V.J.P. Vilar, J.L. Faria, P. Falaras, A.M.T. Silva, Appl. Catal. B 147 (2014) 65–81.
[29] H.X. Li, Z.F. Bian, J. Zhu, Y.N. Huo, H. Li, Y.F. Lu, J. Am. Chem. Soc. 129 (2007) 4538–4539.
[30] G. Louarn, M. Lapkowski, S. Quillard, A. Pron, J.P. Buisson, S. Lefrant, J. Phys. Chem. 100 (1996) 6998–7006.
[31] M. Tgowska, B. Palys, K. Jackowska, Synth. Metal 142 (2004) 223–229.
[32] M. Baibarac, M. Lapkowski, A. Pron, S. Lefrant, I. Baltog, J. Raman Spectrosc. 29 (1998) 825–832.
[33] B.J. Palys, J. Bukowska, K. Jackowska, J. Electroanal. Chem. 428 (1997) 19–24.
[34] M.A. Centeno, M. Paulis, M. Montes, J.A. Odriozola, Appl. Catal. B 61 (2005) 177–183.
[35] F.X. Xiao, F.C. Wang, X.Z. Fu, Y. Zheng, J. Mater. Chem. 22 (2012) 2868–2877.
[36] W. Göpel, J.A. Anderson, D. Frankel, M. Jaehnig, K. Phillips, J.A. Schäfer, G. Rocker, Surf. Sci. 139 (1984) 333–346.
[37] Y. Chen, B. Zhu, M. Yao, S. Wang, S. Zhang, Catal. Commun. 11 (2010) 1003–1007.
[38] Y. Huang, D. Li, J. Li, Chem. Phys. Lett. 389 (2004) 14–18.
[39] E.T. Kang, K.G. Neoh, Y.K. Ong, K.L. Tan, B.T.G. Tan, Macromolecules 24 (1991) 2822–2828.
[40] G. Sebastian, K. Anna, F. Mats, L. Krzysztof, J.L. Jerzy, Solid State Ionics 179 (2008) 2234–2239.
[41] C.B. Bruce, S. Peter, Chem. Mater. 9 (1997) 1949–1953.
[42] M. Date, M. Haruta, J. Catal. 201 (2001) 221–224.
[43] R. Si, J. Liu, K. Yang, X. Chen, W. Dai, X. Fu, J. Catal. 311 (2014) 71–79.
[44] H.B. Fu, T-G. Xu, S.B. Zhu, Y.F. Zhu, Environ. Sci. Technol. 42 (2008) 8064–8069.
[45] S.Y. Zhu, S.J. Liang, Q. Gu, L.Y. Xie, J. Wang, Z. Ding, P. Liu, Appl. Catal. B 119/120 (2012) 146–155.
[46] H. Zhang, X. Lv, Y. Li, Y. Wang, J. Li, ACS Nano 4 (2010) 380–386.
[47] W.X. Dai, X.P. Zheng, H.Y. Yang, X. Chen, X.X. Wang, P. Liu, X.Z. Fu, J. Power Sources 188 (2009) 507–514.
[48] J. Liu, R. Si, H. Zheng, Q. Geng, W. Dai, X. Chen, X. Fu, Catal. Commun. 26 (2012) 136–139.
[49] H.C. Liu, A.I. Kozlov, A.P. Kozlova, T. Shido, K. Asakuray, Y. Iwasawa, J. Catal. 185 (1999) 252–264.